Highly Sensitive and Selective Field-Effect-Transistor NonEnzyme Dopamine Sensors Based on Pt/Conducting Polymer Hybrid Nanoparticles

*Jun Seop Lee, Jungkyun Oh, Sung Gun Kim, and Jyongsik Jang**

Dopamine (DA), as one of catecholamine family of neurotransmitters, is crucially important in humans owing to various critical effects on biometric system such as brine circuitry, neuronal plasticity, organization of stress responses, and control of cardiovascular and renal organizations. Abnormal level of dopamine in the central nervous system causes several neurological diseases, e.g., schizophrenia, Parkinson's disease, and attention deficit hybperactivity disorder (ADHD)/attention deficit disorder (ADD). In this report, we suggest the fabrication of nonenzyme field effect transistor (FET) sensor composed of immobilized Pt particle decorated conducting-polymer (3-carboxylate polypyrrole) nanoparticles (Pt_CPPy) to detect dopamine. The hybrid nanoparticles (NPs) are produced by means of facile chemical reduction of pristine CPPyNP-contained Pt precursor ($PtCl_4$) solution. The Pt_CPPys are then immobilized on an amine-functionalized ($–NH_2$) interdigitated-array electrode substrate, through the formation of covalent bonds with amine groups (–CONH). The resulting Pt_CPPy-based FET sensors exhibit high sensitivity and selectivity toward DA at unprecedentedly low concentrations (100×10^{-15} M) and among interfering biomolecules, respectively. Additionally, due to the covalent bonding involved in the immobilization process, a longer lifetime is expected for the FET sensor.

1. Introduction

Neurotransmitters (NTs) are chemical messengers through secretion from one neuron to the next until binding onto specific receptors located on the membranes of target cell.[1–5] Among various NTs, dopamine (DA) has been widely studied since 1950s due to its important role in the functions of central nervous system, renal, hormonal, and cardiovascular system.[6–8] In particular, abnormal level of DA is believed to be associated with certain neurological disorders known as sleeping and eating disorders, Parkinson's disease, and addictive behaviors associated with drug abuse.[9–12] However, the clinical concentration of DA is very low; for example, the DA levels in plasma, urine, and single adrenal chromaffin cell are in the range of nM (10^{-9} M), μM (10^{-6} M), and fM (10^{-15} M), respectively.[13–15] Therefore, rapid and sensitive detection of DA in biological system is important for the routine analysis and diagnosis of neurological disorders. Several analytical methods have been conducted for detection DA at low concentrations.[16–20] Among them, chromatographic techniques are commonly used for DA detection through high-pressure liquid chromatography (HDLC) and gas chromatography coupled with mass spectrometry (GC–MS).[17,18] However, these chromatographic techniques require sample pretreatment and complex equipment. Enzymatic-assay-based methods have also attracted considerable attention due to their high sensitivity for DA and comparable low cost.[21,22] However, these techniques are not used as frequently owing to accurate DA detection depends strongly on the quality

J. S. Lee, J. Oh, S. G. Kim, Prof. J. Jang
School of Chemical and Biological Engineering
College of Engineering
Seoul National University
599 Gwanangno, Gwanakgu, Seoul 151–742, South Korea
E-mail: jsjang@plaza.snu.ac.kr

DOI: 10.1002/smll.201403263

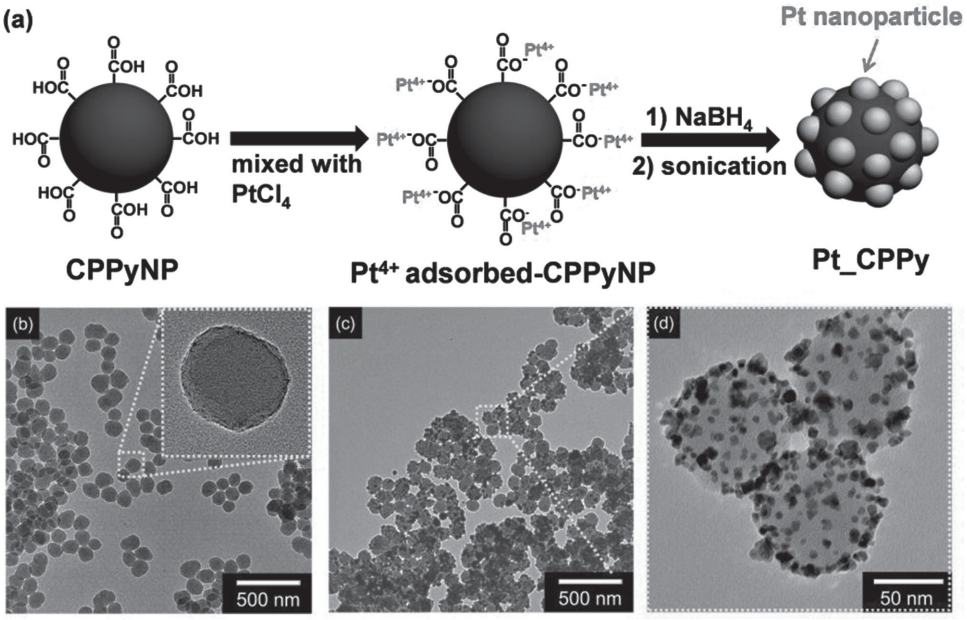

Figure 1. a) Illustrative diagram of the sequential fabrication steps for Pt particle decorated polypyrrole-3-carboxylated nanoparticles (Pt_CPPys). b) Transmission electron microscopy (TEM) images of pristine CPPyNPs (inset: enlarged CPPyNP). c) Low- and d) high-magnified TEM images of Pt_CPPys.

of the prepared enzyme and nonspecific binding to analytes having a similar structure. In this regard, electrochemical sensing technique based on field effect transistors (FETs) for dopamine detection is an attractive method due to low cost, easy operation, fast response, high sensitivity, and feasibility of miniaturization.[23,24]

Conducting polymers (CPs) (e.g., polypyrrole (PPy), polyaniline (PANI), and polythiophene (PT)) displayed interesting chemical and physical properties due to their conjugated polymer backbone comprising alternating single and double bonds.[25–30] Due to their unique properties, CPs have been used as sensor transducers with inherent electronic, optic, and mechanical transducer mechanisms.[31–35] To enhance sensitivity, considerable effort has focused on the fabrication of nanometer-scale CPs due to their beneficial characteristics, such as small size, high surface-to-volume ratio, and amplified signals.[36–38] Recently, several studies have focused in enhancing sensing ability through introduction inorganic materials (i.e., noble metal and metal oxide) in the CP structure to maximize interaction between transducers and target analytes.[39,40] For example, copper (Cu)-modified poly (3,4-ethylenedioxythiophene) (PEDOT) layers were synthesized to apply dopamine detection.[41] However, fabrication of this material as nanostructure is difficult due to aggregation of each component.

Herein, we report the fabrication of a FET-type nonenzyme sensor to detect the one of NT known as DA. The FET sensor is comprised of platinum particle decorated carboxylated polypyrrole nanoparticles (Pt_CPPy) conjugated on the electrode substrate. On account of formation of Pt nanoparticles on the pristine CPPy surface, the active surface area of Pt_CPPys is larger than that of pristine carboxylated polypyrrole nanoparticles (CPPyNPs). As a result, the interaction between the analyte and Pt_CPPy-based transducer is enhanced. Binding CPPyNPs on the FET substrate and decorated Pt particles result in a strong affinity between the Pt and dopamine, thus providing a nonenzyme-FET platform stable for electronic control. Field-induced sensitivities to various dopamine concentrations are observed, eventually leading to the recognition of dopamine at unprecedentedly low concentrations (100×10^{-15} M). Furthermore, this FET-type nonenzyme sensor exhibits high selectivity to the target analyte among molecules with interfering biomolecules (uric acid (UA), ascorbic acid (AA), epinephrine (EP), and norepinephrine (NE)); in addition, its lifetime is relatively long compared with other enzymatic biosensors.

2. Results and Discussion

2.1. Fabrication of Pt Decorated CPPyNPs

Figure 1a suggests the schematic diagram of the platinum nanoparticle decoration on the CPPyNP surface through chemical reduction and following ultrasonication process. As shown in Figure 1b, aggregate-free 60 nm diameter of CPPyNPs was prepared using a monodisperse method, as discussed in our previous work.[42,43] The CPPyNPs were stirred in different concentration of $PtCl_4$ aqueous solutions at room temperature to induce covalent bonding between the Pt^{4+} ions and the negative charge of the O atom of the carboxylate group in the CPPy structure.[44] A small amount of $NaBH_4$ was added to the mixed CPPyNP solutions with ultrasonication for 2 h in order to reduce Pt^{4+} ions to Pt nanoparticles. Figure 1c,d shows the Pt_CPPys decorated with ≈10 nm diameters of uniformly dispersed Pt particles on the surface.

Furthermore, the size and density of the decorated Pt nanoparticles were controlled by the concentration of the

DOI: 10.1002/smll.201403263

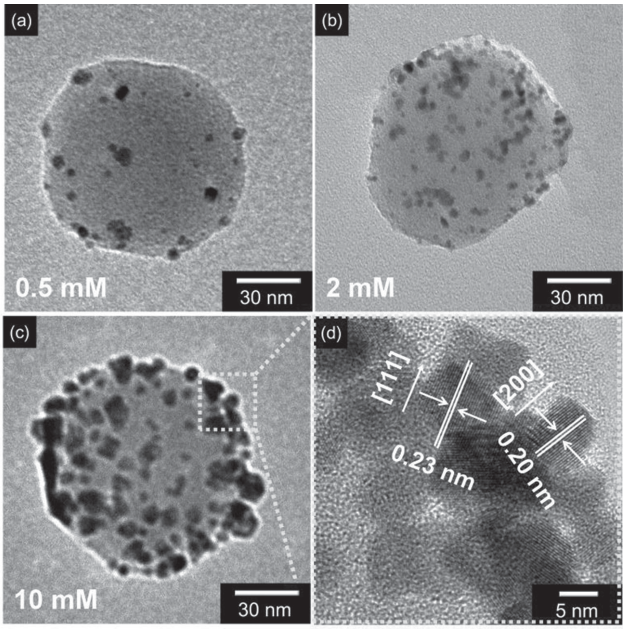

Figure 2. TEM images of Pt_CPPys with different concentrations of $PtCl_4$ solutions: a) 0.5×10^{-3} M (Pt_CPPy_0.5), b) 2×10^{-3} M (Pt_CPPy_2), and c) 10×10^{-3} M (Pt_CPPy_10). d) HR-TEM image of Pt particles on the Pt_CPPy_10 surface.

$PtCl_4$ aqueous solution, which varied from 0.5×10^{-3} to 20×10^{-3} M. The nanostructures of the hybrid CPPys with 0.5×10^{-3}, 2×10^{-3}, 10×10^{-3}, 15×10^{-3}, and 20×10^{-3} M $PtCl_4$ solutions are denoted as Pt_CPPy_0.5, Pt_CPPy_2, Pt_CPPy_10, Pt_CPPy_15, and Pt_CPPy_20, respectively. **Figure 2** shows transmission electron microscopy (TEM) and high-resolution transmission electron microscopy (HR-TEM) images of the hybrid CPPys with increasing precursor concentration. At low concentration (0.5×10^{-3} M), ≈5 nm diameter Pt particles sparsely decorate on the surface. The size and density of decorated Pt particles are increased (≈10 nm) until 10×10^{-3} M of $PtCl_4$ solution. However, over the 10×10^{-3} M $PtCl_4$ concentration, Pt particles formed large scale structure rather than decorated on the CPPy surface, as shown in the Figure S1, Supporting Information. The HR-TEM image of Pt indicates interplanar spacings 0.23 nm and 0.20 nm for the (111) and (200) of face centered cubic (FCC)-Pt and confirms growth of pure crystalline nanoparticles following treatment (Figure 2d). Additionally, to determine the crystallinity and composition of the particles, X-ray diffraction (XRD) using a JCPDS 00–004–0802 system and X-ray photoelectron spectroscopy (XPS) were used, respectively (Figure S2, Supporting Information).

2.2. Fabrication of Pt_CPPy FET Sensor Electrodes

The stability in the liquid-ion solution is critical factor in the fabrication of highly sensitive nonenzyme FET sensor electrodes. To improve stability, the immobilization of the transducer on the sensor electrode is achieved via the covalent bonding of functional groups. **Figure 3** provides a schematic diagram of the procedure for the Pt_CPPy based nonenzyme

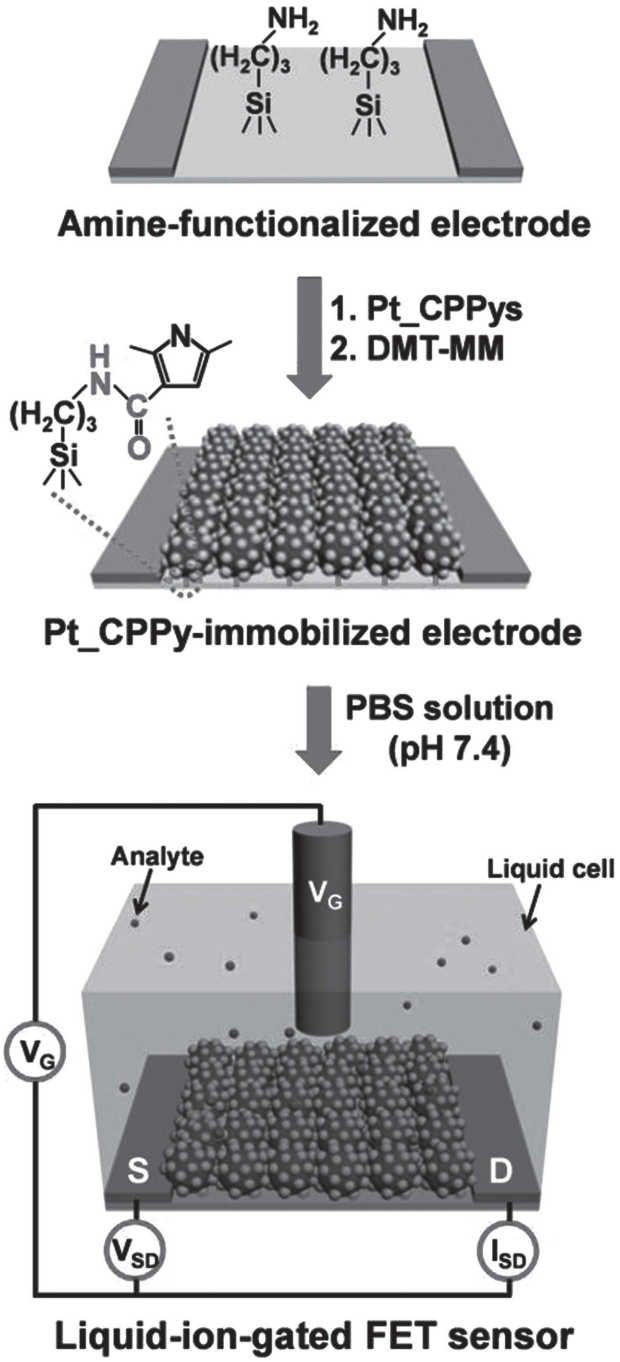

Figure 3. Schematic diagram of the liquid-ion-gated FET with the immobilized Pt_CPPy arrays on the IDA electrode.

FET sensor configuration. An interdigitated microelectrode array (IDA), composed of pairs of 25 lines of gold fingers on the glass plate, was used as immobilization substrate of Pt_CPPys (Figure S3, Supporting Information). The IDA glass substrate was treated with 3-aminopropyltrimethoxysilane (APS) to functionalize the surface with amine groups ($-NH_2$). Subsequently, the Pt_CPPys were anchored to the substrate through a condensation reaction between the carboxyl group (–COOH) of the NPs and the $-NH_2$ of the substrate involving the condensing agent (4-(4,6-dimethoxy-1,3,5-triazin-2-yl)-4-methylmorpholinium chloride (DMT-MM)).[45]

DOI: 10.1002/smll.201403263

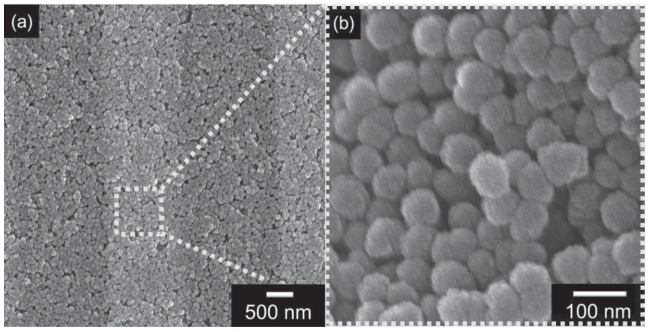

Figure 4. a) Low- and b) high-resolution FE-SEM images of immobilized arrays of the Pt_CPPys on the IDA substrate.

The carboxyl group of the Pt_CPPys facilitated the formation of a compact NP array on the substrate. As a result, Pt_CPPys were immobilized on the electrode substrate, and they demonstrated outstanding stability against environmental perturbation. **Figure 4** shows field-effect scanning electron microscopy (FE-SEM) images of the ordered packing on the IDA substrate. The arrays of ordered, packed hybrid NPs were clearly observed within the IDA. Then, the Pt_CPPy-immobilized IDA was formed FET-sensor platform with phosphated buffer saline (PBS) solution (pH 7.4) as electrolyte. In the FET configuration, two gold IDA bands were the source (S) and drain (D) electrodes and gate electrode was immersed in the electrolyte. The gate potential (V_G) was applied to the source electrode through a PBS solution. The distance between electrodes was fixed at 2 mm based in the resistivity of the PBS solution.

2.3. Characterization of Pt_CPPy FET Sensor Electrodes

To characterize the electrical properties of the Pt_CPPys in the liquid phase, a FET configuration was constructed using an electrolyte as a liquid-ion gate. Current–voltage (*I–V*) curves were used to evaluate the electrical contact of the Pt_CPPys on the IDA substrate. **Figure 5**a shows the I_{SD}–V_{SD} characteristics (V_G = 0) of the various Pt_CPPys with different amount of Pt particle decoration. Pt_CPPys exhibit linearity (i.e., ohmic contact) for voltage range from –0.1 to 0.1 V, as opposed to the nonlinearity exhibition by Schottky barriers with poor electrical contact at the electrode. The *dI*/*dV* values of the electrodes increase as enhancing amount of Pt nanoparticles on the CPPy surface due to Pt particles enhance conductivity of CPPy particles. Furthermore, the dependence of the source–drain current (I_{SD}) with V_G variation (–20–100 mV) was investigated at a constant scan rate (10 mV s^{-1}) of source–drain voltage (V_{SD}) to verify the charge transport properties of Pt_CPPys in the FET configuration. Figure 5b displays a plot of the I_{SD} versus V_{SD} for varying V_G for Pt_CPPy_10 electrode. The I_{SD} increases negatively with negative enhancing V_G, indicating p-type (hole–transport) behavior, caused by an increase in the oxidation level of the polymer chains. Additionally, other hybrid CPPyNPs (Pt_CPPy_0.5 and Pt_CPPy_2) suggest similar tendency except I_{SD} amounts with varying V_G (Figure S4, Supporting Information). However, Pt_CPPy_15 and Pt_CPPy_20 display

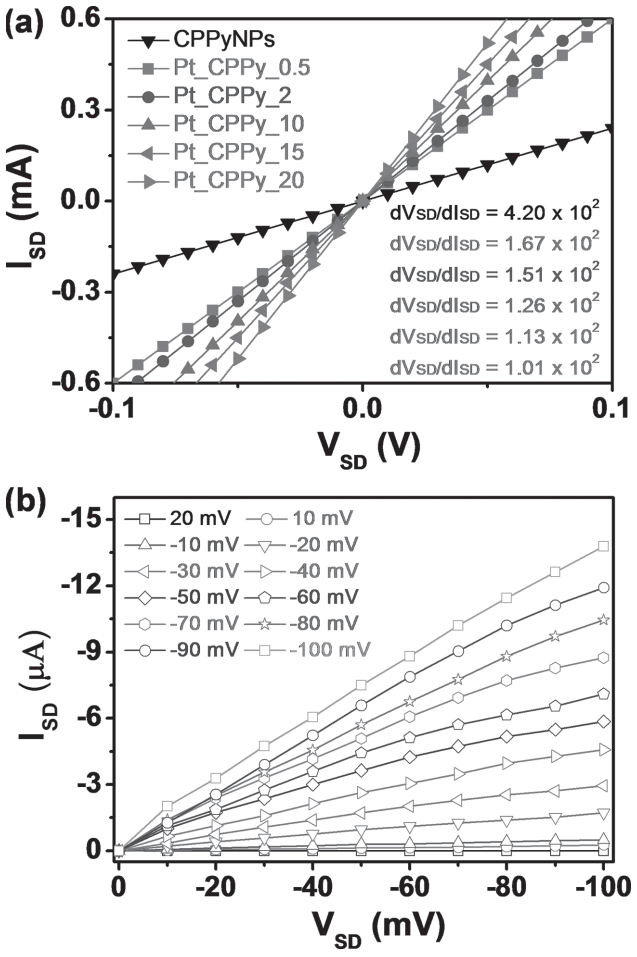

Figure 5. a) Source-drain current–voltage (I_{SD}–V_{SD}) curves without gate potential (V_G) comparison of the IDA electrodes based on different Pt_CPPys (black: pristine CPPyNPs; red: Pt_CPPy_0.5; blue: Pt_CPPy_2; green: Pt_CPPy_10; pink: Pt_CPPy_15; yellow: Pt_CPPy_20). b) Source–drain current versus source–drain voltage (I_{SD}–V_{SD}) characteristics of an Pt_CPPy_10 FET electrode for varying V_G ranging from 20 to –100 mV in 10 mV steps (V_{SD} scan rate: 10 mV s^{-1}).

destruction of p-type charge transport properties in the FET configuration owing to excess amount of Pt particles in the hybrid structure limits semi-conductive function of CPPy particles (Figure S5, Supporting Information). Consequently, the dependence of I_{SD} on V_G is confirmed that proper amount of Pt contained Pt_CPPy FETs could be effectively used as an electrochemical sensor for detecting analytes in solution. The liquid-ion gate is capable of achieving increased transconductance, due to the intimate contact between the NPs and the gate, compared with conventional back-gating.

2.4. Real-Time Responses of Pt_CPPy FET Sensor Electrodes

The uniformly immobilized Pt_CPPys on the FET sensor electrode rapidly detect dopamine molecules at room temperature. The sensing mechanism of the hybrid CPPyNPs is described as shown in **Figure 6**. The CPPy surface is adsorbed to dopamine molecules by pi–pi interactions through conjugated five membered ring of CPPy and six membered

DOI: 10.1002/smll.201403263

small NANO MICRO

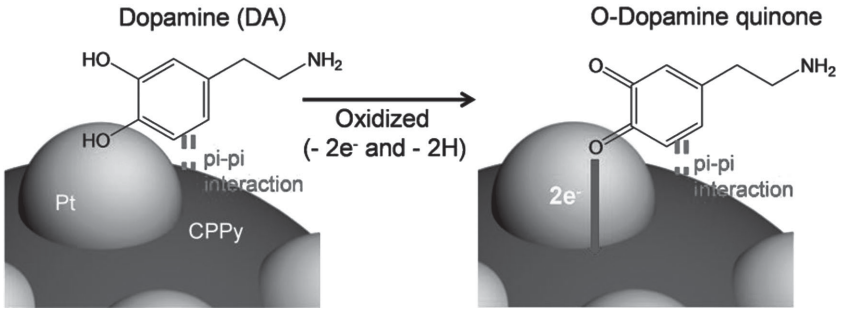

Figure 6. Dopamine molecule detection mechanism of Pt_CPPy FET sensors at room temperature.

benzene ring of dopamine structure. The adsorbed dopamine is electro-oxidized to O-dopaminequinone at the surface of the Pt particles through catalytic effect and electrons, originated from dopamine, are transferred to CPPy, leading to a decrease in the number of holes in the CPPy structure and diminishing I_{SD} (because CPPy acts as a p-type transducer).

To investigate the sensing characteristics of the liquid-ion-gated Pt_CPPy FET, the I_{SD} was monitored in real time at a V_G of 10 mV (V_{SD} = 10 mV), a low operating voltage, upon the addition of various concentration of dopamine. **Figure 7**a shows the real-time response of the Pt_CPPy FET sensors with different decorated Pt particle amounts as a function of DA sensors. Upon each addition of DA, the I_{SD} decreases rapidly over a 1 s period before its saturated value. The sensitivity of the Pt_CPPy FETs increases as the enhancing Pt decoration amounts; that is, the Pt_CPPy FET made from the Pt_CPPy_10 is capable of detecting dopamine concentrations as low as 100×10^{-15} M at room temperature. The larger-amount of Pt particles have a higher density of chemical functionality (degree of Pt catalytic activity), compared with less Pt decorated CPPyNPs. Therefore, a better sensitivity is achieved with large amount of Pt particles as a result of the enhancing catalytic activity to the oxidation of dopamine molecules. Figure 7b shows the changes in sensitivity as a function of Pt particle density for the Pt_CPPys, with respect to dopamine concentration. The sensitivity (S) is determined from the saturation point of the normalized current change ($(\Delta I/I_0)_{SD} \times 100$), measured 10 s after the dopamine addition. At low concentrations ($<100 \times 10^{-15}$ M), the Pt_CPPy FET sensors show nonlinear changes in sensitivity. In contrast, linear behavior is observed over a wide concentration range (100×10^{-15} M–1×10^{-9} M).

The selectivity of the Pt_CPPy_10 FET towards the dopamine molecule was investigated for four organic molecules: AA/UA that are present together in some biological tissues with DA and EP/NE that have similar molecular structure to DA (**Figure 8**a). The Pt_CPPy sensor shows no significant I_{SD} changes with the addition of each nontarget molecules (100×10^{-12} M: AA, UA, and EP; 50×10^{-12} M: EP): however, considerable I_{SD} changes are evident upon the addition of 100×10^{-15} M dopamine (Figure 8b). Additionally, to further confirm the selectivity of the FET sensors, real-time responses were conducted with the addition nontarget molecule mixtures (100×10^{-12} M: AA, UA, and EP; 50×10^{-12} M: EP); some of the mixtures contained 100×10^{-15} M dopamine, while other mixtures without dopamine. Figure 8c shows significant signal changes after the addition of mixtures containing dopamine, compared with the signal obtained for mixtures without dopamine. The pi–pi interaction between phenyl structure of DA and CPPy structure is attributed to the easy adsorbed DA molecules to the surface of Pt_CPPy-based electrode. On the other hand, AA and UA exhibit weaker adsorbed interactions than DA molecules due to absence of phenyl group in the molecular structure. Figure S6, Supporting Information, suggests pi–pi interaction analysis of each biomolecules using XPS spectra. However, despite of similar structure to DA, EP and NE display lower sensitivity than DA. The additional functional groups (–OH and $–CH_3$)

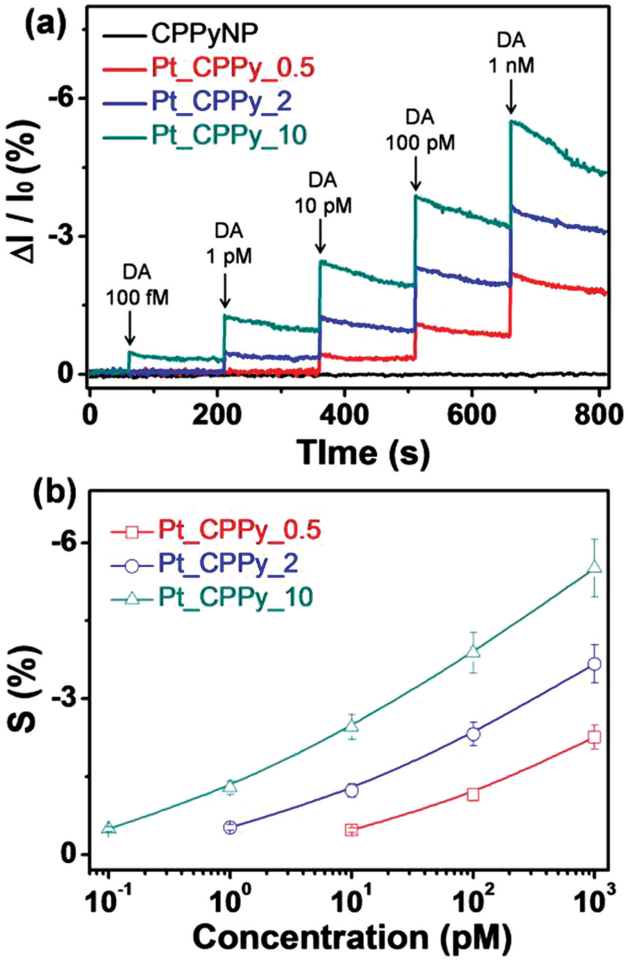

Figure 7. a) Real-time response for the FETs comprising various Pt particle densities of Pt_CPPys, with normalized current changes ($\Delta I/I_0 = (I - I_0)/I_0$, where I_0 is the initial current and I is the instantaneous current). b) Calibration curves of FETs comprising various Pt particle densities of Pt_CPPys as a function of dopamine concentration (S indicates the normalized current change after 10 s of dopamine exposure). Black, red, blue, and green represent FETs originate from the pristine CPPyNPs, Pt_CPPy_0.5, Pt_CPPy_2, and Pt_CPPy_10, respectively (V_G = 10 mV, V_{SD} = 10 mV).

DOI: 10.1002/smll.201403263

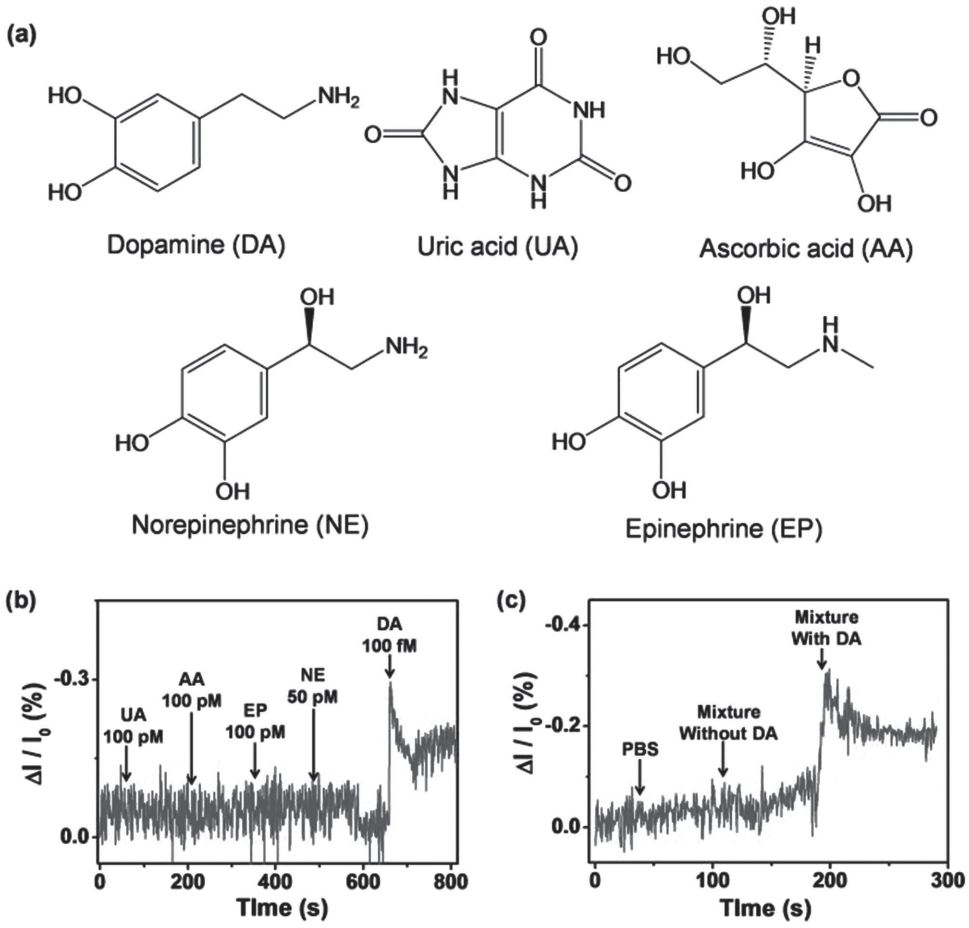

Figure 8. a) Molecular diagram of the different biomolecules. b) Selectivity responses of the Pt_CPPy FET sensors toward nontarget (ascorbic acid (AA), uric acid (UA), epinephrine (EP), and norepinephrine (NE)) and target (dopamine (DA)) analytes. c) Real-time response of the nonenzyme sensor for various analytes, before and after being mixed with dopamine (V_G = 10 mV, V_{SD} = 10 mV).

at ethylamine group enlarged size of biomolecules, so it might be restricted pi–pi interactions with CPPy surface and catalytic effect of Pt particles. As a result, the Pt_CPPy FET sensor exhibits high selectivity to the dopamine molecules in presence of excess interferents.

The main advantage of the chemical-bonding-based FET system is the repeated use (i.e., a longer lifetime); in contrast, adsorption-based systems that require washing/rinsing process for reuse. **Figure 9** shows an estimation of the stability of the FETs based on Pt_CPPys of various Pt densities over several weeks. To confirm stability, the Pt_CPPy FETs were stored in a sealed vessel at 25 °C for 4 weeks under air-dried conditions. The response (S) of the various Pt_CPPy FETs is displayed with 100×10^{-12} M dopamine concentration. Under this condition, the S maintain after 4 weeks due to following reasons. First, the Pt_CPPy FET sensor systems are not concerned enzymatic bioreceptors (e.g., aptamer and antibody) that caused inactivation at harsh conditions. Second, covalent chemical bonding (amide bond) between CPPyNPs and sensor electrodes prohibits destruction of the nanoparticle arrays. Furthermore, the Pt_CPPy FETs maintain their other sensing abilities, such as selectivity and minimum detectable level (MDL) of dopamine without any decrease in the response. Additionally, the morphology of Pt_CPPys remains after DA detection for four weeks (Figure S7, Supporting Information). Therefore, the decorated Pt particles on the CPPy surface also maintain after DA detection process.

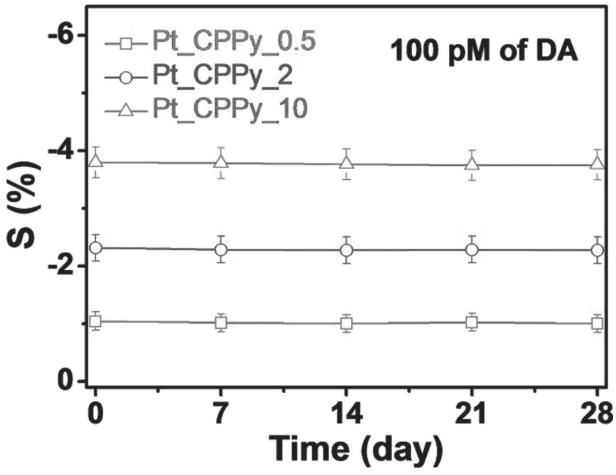

Figure 9. Sensing performance comparison of various hybrid CPPyNP-FET sensors during 4 weeks of storage. Measurements were obtained at 1 week intervals. The hybrid CPPyNPs are Pt_CPPy_0.5 (red), Pt_CPPy_2 (blue), and Pt_CPPy_10 (green), respectively.

DOI: 10.1002/smll.201403263

3. Conclusions

In summary, we fabricated Pt_CPPy FET sensors using chemical reduction and immobilization of the Pt_CPPys on the electrode surface. The decorated Pt particles enhance oxidation amount of dopamine, increasing sensitivity to dopamine molecules. As a result, the Pt_CPPy FET sensors exhibit ultrahigh sensitivity (100×10^{-15} M) to dopamine, 10^2–10^3 times higher than that of other nonenzyme sensors. Moreover, the Pt_CPPy sensor displays selectivity to the dopamine molecule, as well as a long lifetime (4 weeks in this study) with respect to the repeated use of the sensor. The reusability properties of the sensor are attributed to the covalent bonding used in the immobilization process and without bioreceptors. Thus, this study demonstrates an effective method for fabricating FET sensors exhibiting high sensitivity, using noble metal decorated conducting polymer hybrid nanomaterials.

4. Experimental Section

Materials: Poly(vinyl alcohol) (PVA, Mw 9000), $FeCl_3$ (97%), and $PtCl_4$ (99%) were purchased from Aldrich Co. and used without further purification. Pyrrole (98%) and pyrrole-3-carboxylic acid were obtained from Aldrich and Acros Organics. Dopamine (DA), ascorbic acid (AA), uric acid (UA), epinephrine (EP), and norepinephrine (NE) were acquired from Sigma Co.

Fabrication of Pt_CPPys: As the starting material, 60 nm of uniform carboxylated polypyrrole nanoparticles (CPPyNPs) were prepared with PVA, $FeCl_3$, and mixture of pyrrole and pyrrole-3-carboxylic acid monomers (molar ratio of pyrrole : pyrrole-3-carboxylic acid = 30:1), as described in our previous work.[42,43] The prepared CPPyNPs were mixed with various concentration (0.5×10^{-3}–20×10^{-3} M) of $PtCl_4$ aqueous solutions. Then, 0.01 g of $NaBH_4$ was added to the mixed CPPyNP solution with ultrasonication for 2 h to decorate Pt nanoparticles on the CPPyNP surface. The subsequent solution was precipitated with ethanol several times and then dried at 70 °C for 12 h.

Fabrication of Pt_CPPy Nonenzyme FET Sensor: To construct the nonenzyme FET sensor, IDA electrode was treated with 5 wt% aqueous amino-silane (3-aminopropyltrimethoxysilane, APS) for 6 h to introduce amino groups to the electrode surface. Then, the treated electrode was exposed to a mixture of 0.1 wt% Pt_CPPy aqueous solution (40 μL) and 1 wt% 4-(4,6-dimethoxy-1,3,5–2-yl)-4-methylmorpholinium chloride (DMT-MM) aqueous solution (40 μL) for 12 h. Afterward, the Pt_CPPys immobilized electrode was rinsed with distilled water and dried at room temperature.

Electrical Measurement of the Pt_CPPy Nonenzyme FET Sensor: All electrical measurements were conducted using Keithley 2612A source meter and probe station (MS TECH, Model 4000) in pH 7.4 of PBS solution. To utilize the solution-based measurement, a solution chamber (volume: 200 μL) was designed and used. The change in the current was as follows

$$\left[\frac{\Delta I}{I_0}\right]_{SD}(\%) = \frac{(I - I_0)}{I_0} \times 100 \quad (1)$$

where I_0 represents the initial current, and I is the measured real-time current.

Instruments: TEM and HRTEM images were obtained with JEOL JEM-200CX and JEOL JEM-3010 microscopes, respectively. A JEOL 6700 instrument was used to acquire FE-SEM images. X-ray diffraction (XRD) and X-ray photoelectron spectroscopy (XPS) spectra were recorded using M18XHF SRA (MAC Science Co.) and Axis-His (KRATOS), respectively.

Supporting Information

Supporting Information is available from the Wiley Online Library or from the author.

Acknowledgements

This research was supported by the National Research Foundation of Korea (NRF) grant funded by the Korea government (MEST) (Grant No. 2011–0017125).

[1] T. Pradhan, H. S. Jung, J. H. Jang, T. W. Kim, C. Kang, J. S. Kim, *Chem. Soc. Rev.* **2014**, *43*, 4684.
[2] T. C. Sudhof, *Neuron* **2013**, *80*, 675.
[3] D. L. Robinson, B. J. Venton, M. L. A. V. Heien, R. M. Wightman, *Clin. Chem.* **2003**, *49*, 1763.
[4] F. Mora, S. Segorio, A. D. Arco, M. D. Blas, P. Garrido, *Brain Res.* **2012**, *1476*, 71.
[5] V. Hefco, K. Yamada, A. Hefco, L. Hritcu, A. Tiron, T. Nabeshima, *Eur. J. Pharmacol.* **2003**, *475*, 55.
[6] B. E. K. Swmara, B. J. Venton, *Analyst* **2007**, *132*, 876.
[7] K. Jackowska, P. Krysinski, *Anal. Bioanal. Chem.* **2013**, *405*, 3753.
[8] A. Galvan, T. Wichmann, *Clin. Neurophysiol.* **2008**, *119*, 1459.
[9] J. M. Swanson, N. D. Volkow, *J. Child Psycol. Psychiatry* **2009**, *50*, 180.
[10] J. S. Markowitz, A. B. Straughn, K. S. Patrick, *Pharmacotherapy* **2003**, *23*, 1281.
[11] J. W. Dalley, J. P. Roiser, *Neuroscience* **2012**, *215*, 42.
[12] E. Baldrich, R. Gomez, G. Gabriel, F. X. Munoz, *Biosens. Bioelectron.* **2011**, *26*, 1876.
[13] M. Marinelli, J. E. Mccutcheon, *Neuroscience* **2014**, *28*, 176.
[14] J.-M. Beaulieu, *J. Psychiatry Neurosci.* **2012**, *37*, 7.
[15] J. Zheng, X. Zhou, *Bioelectrochemistry* **2007**, *70*, 408.
[16] N. F. Atta, M. F. El-Kady, *Sens. Actuator B-Chem.* **2010**, *145*, 299.
[17] N. Ye, T. Gao, J. Li, *Anal. Methods* **2014**, *6*, 7518.
[18] A. El-Beqqali, A. Kussak, M. Abdel-Rehim, *J. Sep. Sci.* **2007**, *30*, 421.
[19] B.-R. Li, Y.-J. Hsieh, Y.-X. Chen, Y.-T. Chung, C.-Y. Pan, Y.-T. Chen, *J. Am. Chem. Soc.* **2013**, *135*, 16034.
[20] W.-S. Li, P.-X. Hou, C. Liu, D.-M. Sun, J. Yuan, S.-Y. Zhao, L.-C. Yin, H. Cong, H.-M. Cheng, *ACS Nano* **2013**, *7*, 6831.
[21] T. J. Castilho, A. D. P. T. Sotomayor, L. T. Kubota, *J. Pharm. Biomed. Anal.* **2005**, *37*, 785.
[22] L. Stoica, A. Lindgren-Sjolander, T. Ruzgas, L. Gorton, *Anal. Chem.* **2004**, *76*, 4690.
[23] S. J. Park, H. S. Song, O. S. Kwon, J. H. Chung, S. H. Lee, J. H. An, S. R. Ahn, J. E. Lee, H. Yoon, T. H. Park, J. Jang, *Sci. Rep.* **2014**, *4*, 4342.
[24] S. S. J. Aravind, S. Ramaprabhu, *Sens. Actuator B-Chem.* **2011**, *155*, 679.
[25] J. Jang, J. Ha, J. Cho, *Adv. Mater.* **2007**, *19*, 1772.

[26] B. Yameen, T. Puerckhauer, J. Ludwig, I. Ahmed, O. Altinatas, L. Fruk, A. Colsmann, C. Barner-Kowollik, *Small* **2014**, *10*, 3091.
[27] M. M. Lee, J. Teuscher, T. Miyasaka, T. N. Murakami, H. J. Snaith, *Science* **2012**, *338*, 643.
[28] Z. Guo, H. Liu, C. Jiang, Y. Zhu, M. Wan, L. Dai, L. Jiang, *Small* **2014**, *10*, 2087.
[29] B. Seger, J. McCray, A. Mukherji, X. Zong, Z. Xing, L. Wang, *Angew. Chem. Int. Ed.* **2013**, *52*, 6400.
[30] K. Wang, H. Wu, Y. Meng, Z. Wei, *Small* **2014**, *10*, 14.
[31] P. B. Pernnites, S. K. Venkata, B. D. B. Tiu, A. C. C. Yago, R. C. Advincula, *Small* **2012**, *8*, 1669.
[32] W. Tang, M. Zhang, W. Li, X. Zeng, *Talanta* **2014**, *127*, 262.
[33] H. Yoon, J.-Y. Hong, J. Jang, *Small* **2007**, *3*, 1774.
[34] H. Fan, Z. Guo, L. Gao, Y. Zhang, D. Fan, G. Ji, B. Du, Q. Wei, *Biosens. Bioelectron.* **2015**, *64*, 51.
[35] J. S. Lee, J. Jun, D. H. Shin, J. Jang, *Nanoscale* **2014**, *6*, 4188.
[36] J. Jang, *Adv. Polym. Sci.* **2006**, *199*, 189.
[37] Y. Qian, C. Yu, X. Zhou, P. Ma, S. Wu, L. Xu, J. Shen, *Biosens. Bioelectron.* **2014**, *58*, 237.
[38] H. Yoon, J. Jang, *Adv. Funct. Mater.* **2009**, *19*, 1567.
[39] J. S. Lee, D. H. Shin, J. Jun, J. Jang, *ACS Nano* **2013**, *7*, 10139.
[40] C. Xue, Q. Han, Y. Wang, J. Wu, T. Wen, R. Wang, J. Hong, X. Zhou, H. Jiang, *Biosens. Bioelectron.* **2013**, *49*, 199.
[41] A. Stoyanova, V. Tsakova, *J. Solid State Electrochem.* **2010**, *14*, 1957.
[42] J.-Y. Hong, H. Yoon, J. Jang, *Small* **2010**, *6*, 679.
[43] J. S. Lee, S. G. Kim, J. Jun, D. H. Shin, J. Jang, *Adv. Funct. Mater.* **2014**, *24*, 6145.
[44] L. Qiu, B. Liu, Y. Peng, F. Yan, *Chem. Commun.* **2011**, *47*, 2934.
[45] H. Yoon, S. H. Lee, O. S. Kwon, H. S. Song, E. H. Oh, T. H. Park, J. Jang, *Angew. Chem. Int. Ed.* **2009**, *48*, 2755.

Received: November 3, 2014
Revised: December 9, 2014
Published online:

DOI: 10.1002/smll.201403263